

Variational Quantum Approximate Support Vector Machine With Inference Transfer

Siheon Park¹, Daniel K. Park², and June-Koo Kevin Rhee^{*1,3}

¹School of Electrical Engineering and KAIST Institute for IT Convergence, KAIST, Daejeon, Korea

²Dept. of Applied Statistics & Dept. of Statistics and Data Science, Yonsei University, Seoul, Korea

³Qunova Computing, Inc., Deajeon, S. Korea

*rhee.jk@kaist.edu

Abstract

A kernel-based quantum classifier is the most interesting and powerful quantum machine learning technique for hyperlinear classification of complex data, which can be easily realized in shallow-depth quantum circuits such as a SWAP test classifier. A variational quantum approximate support vector machine (VQASVM) can be realized inherently and explicitly on these circuits by introduction of a variational scheme to map the quadratic optimization problem of the support vector machine theory to a quantum-classical variational optimization problem. Probability weight modulation in index qubits of a classifier can designate support vectors among training vectors, which can be achieved with a parameterized quantum circuit (PQC). The classical parameters of PQC is then transferred to many copies of other decision inference circuits. Our VQASVM algorithm is experimented with toy example data sets on cloud-based quantum machines for feasibility evaluation, and numerically investigated to evaluate its performance on a standard iris flower and MNIST data set. The empirical run-time complexity of VQASVM is estimated to be sub-quadratic on the training data set size, while that of the classical solver is quadratic.

Introduction

Quantum computing opens up new exciting prospects of quantum advantages in machine learning in the sense of sample and computation complexity.¹⁻⁴ One of the foundations for such quantum advantages is the ability to efficiently form and manipulate data in a large quantum feature space, especially with kernel functions used in classification and other classes of machine learning.⁵⁻¹⁴

A recent study has realized a quantum kernel-based classifier model simply with a SWAP test algorithm,^{10,11} which opened up a new class of quantum machine learning with a non-linear feature-space mapping. In this article, we enhance a quantum SWAP test classifier (STC) to realize the mathematical model for the maximum-margin property of SVM, which is achieved

by a variational classical-quantum hybrid algorithm to render an approximate quantum state of support vectors.

Classification is one of the most fundamental machine learning techniques often used such as for pattern recognition. The goal of classification is to infer the most likely class of an unseen data point $\hat{\mathbf{x}} \in \mathbb{C}^N$, given a set of labelled examples (i.e. training data) $\mathcal{S} = \{(\mathbf{x}_i, y_i)\}_{i=0}^{M-1} \subset \mathbb{C}^N \times \{0, 1, \dots, L-1\}$. Although the data is real-valued in practical machine learning tasks, we allow complex-valued data without loss of generality. Support vector machine¹⁵ is the most comprehensive model that helps conceptualizing the basis of supervised machine learning, which classifies data by finding the optimal hyperplane associated with the largest margin between the two classes in a feature space.¹⁶⁻¹⁸ The SVM formulation utilizes a variational method that provides robust binary classification based on a global minimum search guaranteed by convex optimization with kernel functions. Power kernel functions can be used for a non-linear hyperplane classification in a high-dimensional space.¹⁹ In this article, we limit our focus on binary classification where only two classes of the data (i.e. $L = 2$) exist. Multi-class classification can be achieved with a multiple binary SVM consisting of a one-versus-all or one-versus-one scheme.²⁰

A quantum version of SVM has been proposed as Least-Square Quantum Support Vector Machine (LS-QSVM),⁵ which provides an exponential speed up in a sense of computational complexity if applied to ideal quantum machines with the cost of data encoding neglected. However, the LS-QSVM classifier relies on costly subroutines such as the density matrix exponentiation and the quantum matrix inversion,²¹⁻²³ which cannot be implemented with noisy intermediate-scale quantum (NISQ) devices.²⁴

It is important to develop quantum binary classification algorithms that are feasible on near-term quantum technologies of NISQ, such as Hardamard-test classifier (HTC) and swap-test classifier (STC).^{10,11} These classifiers are also kernel-based machine learning models similarly to LS-QSVM, but do not require complex operation such as density matrix exponentiation and quantum matrix inversion, and hence much more feasible than the LS-QSVM. However, STC and HTC treat all training data with a uniform weight in a feature space, and thus there is no optimization to maximize the margin differently from SVM. We develop a quantum machine learning model that combines simplicity of STC in the maximum-margin property of SVM. In this work, we present a variational classical-quantum hybrid supervised machine learning algorithm for swap-test-based binary classification with classical optimization to approximate support vectors. A quantum circuit is used to measure the loss function efficiently while classical optimization is used for the variational method to minimize the loss function. The solution is expected to provide better classification performance than HTC and STC. Moreover, this algorithm does not require density matrix exponentiation or quantum matrix inversion, and hence much more suitable for quantum machine learning on NISQ machines than LS-QSVM.

Result

Support Vector Machine (SVM)

Suppose the data set $\mathcal{S} = \{(\mathbf{x}_i, y_i)\}_{i=0}^{M-1} \subset \mathcal{X} \times \mathcal{Y}$ where data space is $\mathcal{X} \subset \mathbb{C}^N$ and class label space is $\mathcal{Y} = \{-1, 1\}$. We assume that given some feature map $\phi : \mathcal{X} \mapsto \mathcal{H}$, \mathcal{S} is linearly separable in the feature Hilbert space \mathcal{H} . Then there should exist two parallel supporting hyperplanes $\langle \mathbf{w}, \phi(\cdot) \rangle + b = y \in \mathcal{Y}$ that divide training data. The goal is to find these hyperplanes that the margin between them is maximized. To further maximize the margin, linearly separable condition can be relaxed, so that some of the training data can penetrate into the “soft” margin. Since the margin is given as $2/\|\mathbf{w}\|$ by simple geometry, the mathematical formulation of SVM¹³ is given as

$$p^* = \min_{\mathbf{w}, b, \xi} \frac{1}{2} \|\mathbf{w}\|^2 + \frac{C}{2} \sum_{i=0}^{M-1} \xi_i^2 : y_i (\langle \mathbf{w}, \phi(\mathbf{x}_i) \rangle + b) \geq 1 - \xi_i, \quad (1)$$

where slack variable ξ is introduced to represent violation of the data on linearly separable condition. The dual formulation²⁵ of SVM is given as

$$d^* = \max_{\beta \geq 0} \sum_{i=0}^{M-1} \beta_i - \frac{1}{2} \sum_{i,j=0}^{M-1} \beta_i \beta_j y_i y_j k(\mathbf{x}_i, \mathbf{x}_j) - \frac{1}{2C} \sum_{i=0}^{M-1} \beta_i^2 : \sum_{i=0}^{M-1} \beta_i y_i = 0, \quad (2)$$

where the positive semi-definite (PSD) kernel is $k(\mathbf{x}_1, \mathbf{x}_2) = \langle \mathbf{x}_1, \mathbf{x}_2 \rangle$ for $\mathbf{x}_{1,2} \in \mathcal{X}$ and β is a Karush-Kuhn-Tucker multiplier vector consisting of non-negative β_i 's. This formulation employs an implicit feature map with the kernel, and Eq. (2) is a typical formulation of nonlinear soft-margin support vector machine. The global solution β^* is obtained in polynomial time due to convexity.²⁵ After optimization, an optimum bias is recovered as $b^* = y_q (1 - C^{-1} \beta_q^*) - \sum_{i=0}^{M-1} \beta_i^* y_i k(\mathbf{x}_q, \mathbf{x}_i)$ for any $\beta_q^* > 0$. We estimate labels of unseen data with binary classifier:

$$\hat{y} = \text{sgn} \left\{ \sum_{i=0}^{M-1} \beta_i^* y_i k(\mathbf{x}_i, \hat{\mathbf{x}}) + b^* \right\}, \quad (3)$$

In a first-hand principle analysis, the complexity of solving Eq. (2) is $\mathcal{O}(M^2(N + M) \log(1/\delta))$ with the accuracy δ , since a kernel function with complexity of $\mathcal{O}(N)$ is queried $M(M - 1)/2$ times to construct kernel matrix and quadratic programming takes $\mathcal{O}(M^3 \log(1/\delta))$ for finding β^* for non-sparse kernel matrix.⁵ Although the complexity of SVM can be reduced with modern programming methods,^{26,27} it is still higher or equal to $\mathcal{O}(M^2N)$ due to kernel matrix generation and quadratic programming. Thus, a quantum algorithm that evaluates all the terms in Eq. (2) about $\mathcal{O}(MN)$ time and achieves minimum less than $\mathcal{O}(M)$ evaluations would have lower complexity than classical algorithms. We apply two forms of transformations on Eq. (2) to realize the efficient quantum algorithm.

Change of Variable & Bias Regularization

SVM is constrained quadratic programming, which is generally harder than unconstrained programming. Constrained programming is often transformed to unconstrained programming, which is usually realized by adding penalty of violating constraints to the objective function. Although there are well-known methods such as an interior point method, we choose ‘change of variables’ and ‘bias regularization’ to maintain the quadratic form of SVM. Although simply motivated to eliminate constraints, the results seem likely to lead to an efficient quantum SVM algorithm.

For reducing inequality constraints, let us define $B := \sum_{i=0}^{M-1} \beta_i$ and $\boldsymbol{\alpha} := \boldsymbol{\beta}/B$. Then $\boldsymbol{\alpha}$ is an M -dimensional probability vector since $0 \leq \alpha_i \leq 1, \forall i \in \{0, \dots, M-1\}$ and $\sum_{i=0}^{M-1} \alpha_i = 1$. Let us define $W_k(\boldsymbol{\alpha}; \mathcal{S}) := \sum_{i,j=0}^{M-1} \alpha_i \alpha_j y_i y_j k(\mathbf{x}_i, \mathbf{x}_j) + C^{-1} \sum_{i=0}^{M-1} \alpha_i^2$. We substitute variables to Eq. (2):

$$\max_{\boldsymbol{\alpha} \in PV_M} \max_{B \geq 0} \left\{ B - \frac{1}{2} B^2 W_k(\boldsymbol{\alpha}; \mathcal{S}) \right\} : \sum_{i=0}^{M-1} \alpha_i y_i = 0, \quad (4)$$

where PV_M is a set of M -dimensional probability vectors. Since $W_k(\boldsymbol{\alpha}; \mathcal{S}) \geq 0$ for arbitrary $\boldsymbol{\alpha}$ by the property of positive semi-definite kernel, $B^* = 1/W_k(\boldsymbol{\alpha}; \mathcal{S})$ is a partial solution that maximizes Eq. (4) on B . Substituting B^* with Eq. (4), we have

$$\max_{\boldsymbol{\alpha} \in PV_M} \frac{1}{2W_k(\boldsymbol{\alpha}; \mathcal{S})} : \sum_{i=0}^{M-1} \alpha_i y_i = 0. \quad (5)$$

Finally, since maximizing $1/2W_k(\boldsymbol{\alpha}; \mathcal{S})$ is equivalent to minimizing $W_k(\boldsymbol{\alpha}; \mathcal{S})$, we have

$$\tilde{d}^* = \min_{\boldsymbol{\alpha} \in PV_M} \sum_{i,j=0}^{M-1} \alpha_i \alpha_j y_i y_j k(\mathbf{x}_i, \mathbf{x}_j) + \frac{1}{C} \sum_{i=0}^{M-1} \alpha_i^2 : \sum_{i=0}^{M-1} \alpha_i y_i = 0, \quad (6)$$

which is equivalent to Eq. (2). Eq. (6) implies that instead of optimizing M numbers of bounded free parameters $\boldsymbol{\beta}$ or $\boldsymbol{\alpha}$, we can optimize $\log(M)$ -qubits quantum state $|\psi_{\boldsymbol{\alpha}}\rangle$ and define $\alpha_i := |\langle i | \psi_{\boldsymbol{\alpha}} \rangle|^2$. Therefore, if there exists an efficient quantum algorithm that evaluates objective function of Eq. (6) given $|\psi_{\boldsymbol{\alpha}}\rangle$, complexity of SVM would be improved. In fact, in [the later section](#), we propose quantum circuits with the linearly scaling complexity for that purpose.

Introducing l_2 -regularizing bias in Eq. (1) eliminates equality constraint. Motivated from the loss function and regularization perspectives of SVM,²⁸ this technique has been introduced^{29,30} and developed^{31,32} previously, as follows:

$$p^* = \min_{\mathbf{w}, b, \xi} \frac{1}{2} \|\mathbf{w}\|^2 + \frac{\lambda}{2} b^2 + \frac{C}{2} \sum_{i=0}^{M-1} \xi_i^2 : y_i (\langle \mathbf{w}, \phi(\mathbf{x}_i) \rangle + b) \geq 1 - \xi_i, \quad (7)$$

$$d^* = \max_{\boldsymbol{\beta} \succeq 0} \sum_{i=0}^{M-1} \beta_i - \frac{1}{2} \sum_{i,j=0}^{M-1} \beta_i \beta_j y_i y_j \left[k(\mathbf{x}_i, \mathbf{x}_j) + \frac{1}{\lambda} \right] - \frac{1}{2C} \sum_{i=0}^{M-1} \beta_i^2. \quad (8)$$

Note that $k(\cdot, \cdot) + \lambda^{-1}$ is a positive definite. Eq. (8) becomes the same optimization problem as given

$$\tilde{d}^* = \min_{\alpha \in PV^M} \sum_{i,j=0}^{M-1} \alpha_i \alpha_j y_i y_j \left[k(\mathbf{x}_i, \mathbf{x}_j) + \frac{1}{\lambda} \right] + \frac{1}{C} \sum_{i=0}^{M-1} \alpha_i^2 \quad (9)$$

by the change of variables. Since the optimal bias is given as $b^* = \lambda^{-1} \sum_{i=0}^{M-1} \alpha_i^* y_i$ by the Karush-Kuhn-Tucker condition, the classification formula inherited from Eq. (3) is expressed as

$$\hat{y} = \text{sgn} \left\{ \sum_{i=0}^{M-1} \alpha_i^* y_i \left[k(\mathbf{x}_i, \mathbf{x}_j) + \frac{1}{\lambda} \right] \right\}. \quad (10)$$

Eqs. (8) and (9) can be viewed as Eqs. (2) and (6) with a quadratic penalizing term on equality constraint. Thus, Eqs. (1), (2), and (6) are the special cases of Eqs. (7), (8), and (9), respectively, at the limit of $\lambda \rightarrow 0$. However, the numerical simulation on [the later section](#) shows that choosing too small λ and C at the same time hinders learning due to heavy regularization. Note that there are two regularization terms: $\sum_{i=0}^{M-1} \alpha_i^2$ for the slack variables and $(\sum_{i=0}^{M-1} \alpha_i y_i)^2$ for bias.

Variational Quantum Approximate Support Vector Machine

Ansatz $V(\boldsymbol{\theta})$ refers to a unitary quantum gate or circuit that can generate an arbitrary quantum state depending on parameters $\boldsymbol{\theta}$: $|\psi_{\alpha}\rangle = \sum_{i=0}^{M-1} \sqrt{\alpha_i} |i\rangle = V(\boldsymbol{\theta}) |+\rangle$. Amplitude encoding is used ideally: $V(\boldsymbol{\theta}) |+\rangle = \frac{1}{\|\boldsymbol{\theta}\|_1} \sum_{i=0}^{M-1} \sqrt{\theta_i} |i\rangle$. This can preserve the SVM convexity on optimization parameters. However, an amplitude encoding structure is complex,³³ and the required number of parameters is still M .

An advanced quantum algorithm can be constructed if Eqs. (9) and (10) can be computed within $\mathcal{O}(M)$ time. Given probability vector encoded by a PQC (i.e. $\alpha_i = |\langle i | V(\boldsymbol{\theta}) |+\rangle|^2$) the loss, regularizing, and decision functions in Eqs. (9) and (10) can be written in terms of $\boldsymbol{\theta}$:

$$\mathcal{L}_{\phi, \lambda}(\boldsymbol{\theta}; \mathcal{S}) = \sum_{i,j=0}^{M-1} \alpha_i \alpha_j y_i y_j \left[|\langle \phi(\mathbf{x}_i) | \phi(\mathbf{x}_j) \rangle|^2 + \frac{1}{\lambda} \right], \quad (11)$$

$$\mathcal{R}(\boldsymbol{\theta}) = \sum_{i=0}^{M-1} \alpha_i^2, \quad (12)$$

and

$$f_{\phi, \lambda}(\mathbf{x}; \boldsymbol{\theta}, \mathcal{S}) = \sum_{i=0}^{M-1} \alpha_i y_i \left[|\langle \phi(\mathbf{x}_i) | \phi(\mathbf{x}) \rangle|^2 + \frac{1}{\lambda} \right], \quad (13)$$

respectively, where the kernel function is a Hilbert-Schmidt inner product between quantum feature states $|\phi(\cdot)\rangle$.

We propose quantum circuits in Fig. 1 that evaluate $\mathcal{L}_{\phi, \lambda}$, \mathcal{R} and $f_{\phi, \lambda}$ efficiently, inspired by STC.^{10, 11} $\mathcal{U}_{\phi, \mathcal{S}}$ embeds the entire training data set with the corresponding quantum feature map $U_{\phi(\mathbf{x})} |\mathbf{0}\rangle = |\phi(\mathbf{x})\rangle$, so that $\mathcal{U}_{\phi, \mathcal{S}} |i\rangle \otimes |\mathbf{0}\rangle \otimes |0\rangle = |i\rangle \otimes |\phi(\mathbf{x}_i)\rangle \otimes |y_i\rangle$. Therefore, an initial

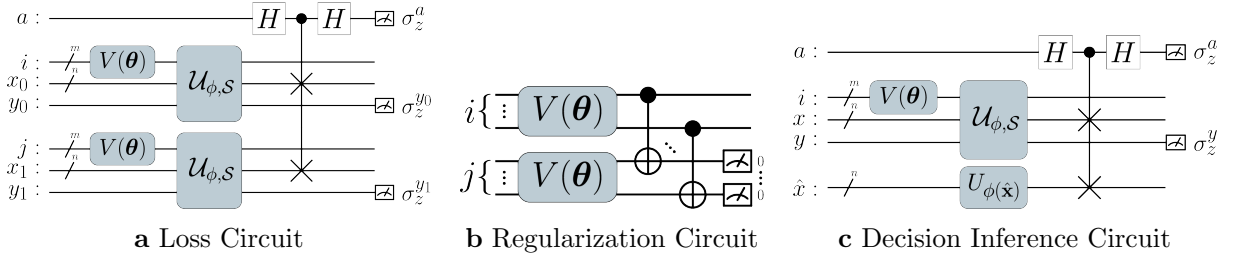


Figure 1: Circuit Architecture of VQASVM. In **a**, all qubits of index register i and j are initialized to $|+\rangle$, and the rest to $|0\rangle$. Ansatz $V(\boldsymbol{\theta})$ is a PQC of $m = \log(M)$ qubits that encodes probability vector $\boldsymbol{\alpha}$. In **a** and **c**, $\mathcal{U}_{\phi, \mathcal{S}}$ embeds a training data set \mathcal{S} with a quantum feature map $U_{\phi(\hat{\mathbf{x}})}$, which embeds classical data $\hat{\mathbf{x}}$ to a quantum state $|\phi(\hat{\mathbf{x}})\rangle$. n denotes the number of qubits for the quantum feature map, which is usually N but can be reduced to $\log(N)$ if amplitude encoding of classical data is used. The complexity of both training and decision circuit is $\mathcal{O}(MN)$. In **b**, the complexity of regularization circuit is $\mathcal{O}(\text{polylog}(M))$.

quantum state after state preparation is

$$|\Psi\rangle = \sum_{i=0}^{M-1} \sqrt{\alpha_i} |i\rangle \otimes |\phi(\mathbf{x}_i)\rangle \otimes |y_i\rangle. \quad (14)$$

We apply a SWAP test and joint σ_z measurement in loss and decision circuits to evaluate $\mathcal{L}_{\phi, \lambda}$ and $f_{\phi, \lambda}$:

$$\mathcal{L}_{\phi, \lambda}(\boldsymbol{\theta}; \mathcal{S}) = \langle \sigma_z^a \sigma_z^{y_1} \sigma_z^{y_2} \rangle_{\boldsymbol{\theta}} + \frac{1}{\lambda} \langle \sigma_z^{y_1} \sigma_z^{y_2} \rangle_{\boldsymbol{\theta}} \quad (15)$$

and

$$f_{\phi, \lambda}(\mathbf{x}; \boldsymbol{\theta}, \mathcal{S}) = \langle \sigma_z^a \sigma_z^y \rangle_{\mathbf{x}; \boldsymbol{\theta}} + \frac{1}{\lambda} \langle \sigma_z^y \rangle_{\mathbf{x}; \boldsymbol{\theta}}. \quad (16)$$

See [Method](#) for specified derivations. $\mathcal{R}(\boldsymbol{\theta})$ can be evaluated as success probability of measuring the $\log(M)$ bit sequence of zeros in the regularization circuit. The asymptotic complexities of loss and decision circuits are linear on the number of training data. $\mathcal{U}_{\phi, \mathcal{S}}$ can be prepared with $\mathcal{O}(MN)$ operations.⁴ See [Method](#) for specific realization used in this article. $V(\boldsymbol{\theta})$ takes $\mathcal{O}(\text{polylog}(M))$ complexity for hardware-efficient PQC encoding and amplitude encoding.^{33,34} A SWAP test takes only $\mathcal{O}(N)$ complexity. Importantly, this model requires only $\mathcal{O}(1)$ qubit measurements. The overall run-time complexity of evaluating $\mathcal{L}_{\phi, \lambda}(\boldsymbol{\theta}; \mathcal{S})$ and $f_{\phi, \lambda}(\mathbf{x}; \boldsymbol{\theta}, \mathcal{S})$ with accuracy ϵ is $\mathcal{O}(\epsilon^{-2}MN)$. Moreover, complexity of evaluating $\mathcal{R}(\boldsymbol{\theta})$ with accuracy ϵ is $\mathcal{O}(\epsilon^{-2}\text{polylog}(M))$, due to two parallel $V(\boldsymbol{\theta})$ s, $\mathcal{O}(\log(M))$ CNOT gates, and success-probability measurement.

Here, we aim to find PQC designs with reduced numbers of parameters since complexity of a gradient-based optimization algorithm is proportional to the number of parameters, which is generally used for solving quadratic programming.^{4,25,28} Given no prior information, the most efficient ansatz design can be a hardware-efficient PQC, which consists of alternating local rotation layers and entanglement layers.^{35,36} In typical applications, the number of parameters is $L \times \text{polylog}(M)$ mainly determined by the number of layers L . We expect that there exists $\boldsymbol{\theta}^*$ such that $\boldsymbol{\alpha}^* \approx |\langle \cdot | V(\boldsymbol{\theta}^*) | + \rangle|^2$ since expressibility of well-designed PQC saturates to that

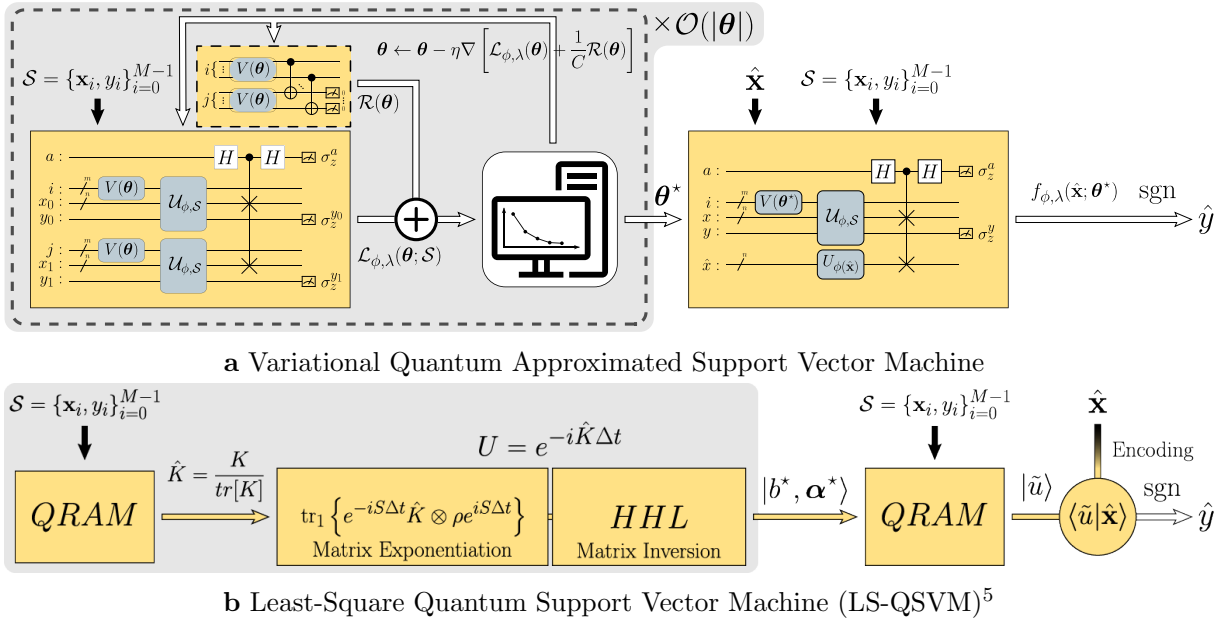


Figure 2: Process of VQASVM compared to LS-QSVM.⁵ In **a** and **b**, the white round boxes represent classical calculations whereas the yellow round boxes represent quantum operations. The white arrows represent the flow of classical data whereas the yellow arrows represent the flow of quantum data. The black arrows represent embedding of classical data. The grey areas indicate the corresponding training phase of each algorithms. In **a**, the regularization circuit in the black dashed box can be omitted for a hard-margin case with $C \rightarrow \infty$.

of Haar distribution with an increasing number of layers.³⁵ In fact, since α^* may not be unique and only the magnitudes of amplitudes of $|\psi_\alpha\rangle$ matters, $V(\theta)$ can well approximate the solution even with the limited expressibility with a fewer number of parameters.

We propose a Variational Quantum Approximate Support Vector Machine (VQASVM) algorithm inspired by quantum approximate optimization algorithm that can reduce the number of parameters PQC designs for certain problems.³⁷ Fig. 2a summarizes the process of VQASVM. We estimate θ^* that minimizes $\mathcal{L}_{\phi,\lambda} + C^{-1}\mathcal{R}$, which is then used for classifying unseen data:

$$\theta^* = \arg \min_{\theta} \mathcal{L}_{\phi,\lambda}(\theta; \mathcal{S}) + \frac{1}{C} \mathcal{R}(\theta), \quad \hat{y} = \text{sgn} \{f_{\phi,\lambda}(\hat{\mathbf{x}}; \theta^*, \mathcal{S})\}. \quad (17)$$

Any unconstrained minimization methods such as gradient descent can be applied to solve the minimization problem. Following a general scheme of a variational quantum algorithm (VQA),³⁸ parameters θ^t at the t -th iteration are updated as $\theta^{t+1} = \theta^t - \eta_t \nabla_{\theta} [\mathcal{L}_{\phi,\lambda}(\theta^t; \mathcal{S}) + C^{-1}\mathcal{R}(\theta^t)]$ by classical processors, whereas the function evaluations for gradients (i.e. by applying parameter-shift rule^{39,40}) are performed on quantum processors. Gradient descent algorithm will converge to a local minimum after $\mathcal{O}(\log(1/\delta))$ iterations with accuracy δ .²⁵ Therefore the run-time complexity of VQASVM is at most $\mathcal{O}(M^2 N \log 1/\delta)$ with accuracy δ , similar to conventional SVM. This complexity can be reduced using hardware-efficient ansatz, comparable to the cost of convexity. In addition, VQASVM requires only $\mathcal{O}(\log(M) + N)$ space whereas classical SVM does $\mathcal{O}(M^2)$.

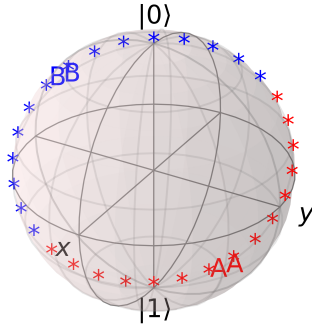
Comparison with Other Methods

The VQASVM method manifests distinctive features from other quantum kernel-based supervised machine learning algorithms. One of the most well-know example is Least-Square Quantum Support Vector Machine (LS-QSVM).⁵ The goal of LS-QSVM is to find hyperplane that minimizes $\frac{1}{2}\|\mathbf{w}\|^2 + \frac{C}{2}\sum_{i=0}^{M-1}(1 - \langle \mathbf{w}, \phi(\mathbf{x}_i) \rangle - b)^2$, which can be transformed to a linear equation by the Karush-Kuhn-Tucker condition.⁴¹ LS-QSVM solves this linear equation using quantum linear solver algorithm proposed by Harrow, Hassidim, and Lloyd (HHL) achieving quantum exponential speed-up,²¹ once we have efficient quantum random access memory (QRAM).² See Fig. 2b. The run-time complexity of LS-QSVM is $\mathcal{O}(\kappa_{\text{eff}}^3 \epsilon^{-3} \log(MN))$ with accuracy ϵ and effective condition number κ_{eff} .

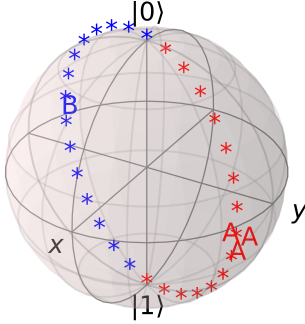
However, we can speculate if practical implementation of LS-QSVM is feasible due to lengthy subroutines such as quantum phase estimation, quantum matrix exponentiation, and inversion. LS-QSVM requires a fault-tolerant universal quantum computer, which is not likely available in the near future. Also, training has to be repeated for each query of an unseen data since the solution of training is in a quantum state, which collapses by the measurements at the end of quantum computation; classification on multiple test data cannot be performed in parallel due to no-cloning theorem. VQASVM can overcome these drawbacks. VQASVM can be realized with much shorter operations; VQASVM circuits are much shorter than HHL circuit on the same moderate system size when decomposed in the same universal gate set. Classification phase of VQASVM can be separated from training phase and performed simultaneously; training results are classically saved and transferred to an decision circuit in other quantum processing units(QPUs).

Other quantum kernel-based algorithms such as variational quantum classifier (VQC) and quantum kernel estimator (QKE) are proposed.⁸ Given quantum feature map $U_{\phi(\mathbf{x})}|\mathbf{0}\rangle = |\phi(\mathbf{x})\rangle$, binary function $f : \{0, 1\}^{\otimes N} \rightarrow \{-1, 1\}$, and ansatz $W(\boldsymbol{\theta})$, VQC estimates a label of data \mathbf{x} to be $\text{sgn}\{\bar{f}(\mathbf{x}; \boldsymbol{\theta}) + b\}$ where $\bar{f}(\mathbf{x}; \boldsymbol{\theta})$ is an empirical average of $f(z)$ such that z is the N -bit measurement result of a quantum circuit $W(\boldsymbol{\theta})|\phi(\mathbf{x})\rangle$ in the computational basis. Parameters $\boldsymbol{\theta}$ and b are trained by variational methods to minimize empirical risk $R_{\text{emp}}(\boldsymbol{\theta}, b) = \frac{1}{|\mathcal{S}|} \sum_{(\mathbf{x}, y) \in \mathcal{S}} \Pr[y \neq \text{sgn}\{\bar{f}(\mathbf{x}; \boldsymbol{\theta}) + b\}]$. Empirically, this requires $\mathcal{O}(MN)$ quantum circuit evaluations.⁴ Although the classification decision of VQC is the same as conventional SVM and VQASVM, VQC is not a convex algorithm unlike SVM and VQASVM. This makes optimization inefficient against local-minima and barren-plateau problems. VQC can have quantum advantage only when the quantum feature map can be computed more efficiently by quantum computing than classical computing.⁸

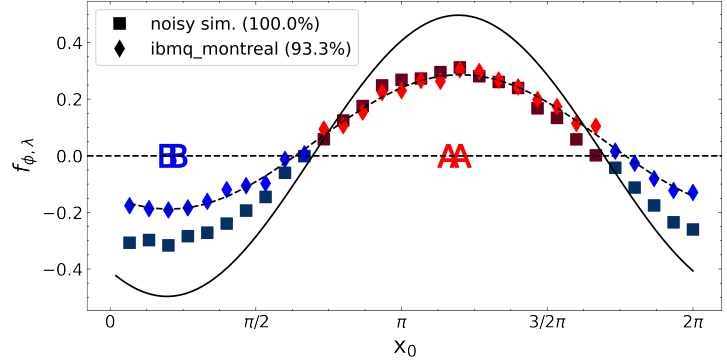
On the other hand, given the true kernel matrix $K_{ij} = |\langle \phi(\mathbf{x}_i) | \phi(\mathbf{x}_j) \rangle|^2$, QKE estimates the kernel matrix elements \hat{K}_{ij} from empirical probability of measuring N -bits zero sequence on a quantum circuit $U_{\phi(\mathbf{x}_i)}^\dagger U_{\phi(\mathbf{x}_j)}|\mathbf{0}\rangle$. The estimated kernel matrix is then used for classical kernel-based algorithms, such as a dual form of SVM. The test kernel matrix for classification is also estimated by the same method. The kernel matrix can be estimated in $\mathcal{O}(\epsilon^{-2}M^4)$ measurements with kernel accuracy $\|K - \hat{K}\| \leq \epsilon$. Thus, although being completely convex,



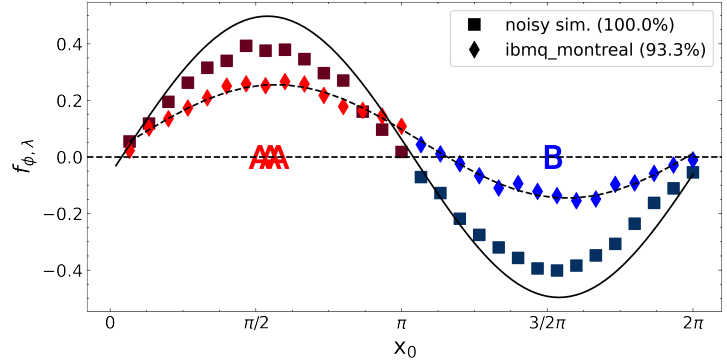
a Balanced data set



c Unbalanced data set



b Balanced data set classification result



d Unbalanced data set classification result

Figure 3: Experimental demonstration on NISQ device($\lambda = 1, C = \infty$). Letters A and B indicate training data sets Data that belong to classes A and B are colored in red and blue, respectively. In **a** and **c**, the balanced and unbalanced toy example data set embedded into a single-qubit. The asterisk markers indicate test data sets. In **b** and **d**, classification results of VQASVM performed on *ibmq_montreal* QPU(diamonds) and simulation with noise(squares), compared to theoretical values(solid line). Letters A and B represent the training data located according to their first feature x_0 , which is the longitudinal coordinate on Bloch sphere. Curved dashed lines are the sine-fitted line of *ibmq_montreal* results. We report the classification accuracy using NISQ device is 93.3% for both toy example data sets.

QKE has a complexity much higher than both VQASVM and classical SVM.⁸

Experiments on IBM Quantum Processors

We demonstrate classification of two different types of toy example data sets using the VQASVM algorithm on NISQ computers. Due to decoherence and the limited number of two qubit gates in NISQ devices, we set the data dimension to $N = 2$ and number of training data to $M = 4$. Our toy example data sets are mapped on a Bloch sphere as shown in Figs. 3a and 3c. The numbers of training data for the two classes A and B are the same for the balanced data set but different for the unbalanced data. The balanced data set is generated as follows. We first randomly choose a greatest circle on the Bloch sphere that passes $|0\rangle$ and $|1\rangle$. Then we randomly choose two opposite points in the circle to be the center of two classes, A and B. Subsequently, four training data are generated close to each class center in order to avoid overlaps between

test data and each others. As a result, we have a good training data set with a maximum margin so that soft-margin consideration is not needed. In addition, thirty test data are generated evenly along the great circle and labelled 1 or -1 according to inner products with the class centers. In this case, VQASVM is simple as $C \rightarrow \infty$ and hence requires no regularization circuit evaluation. The test data set is non-trivial to classify since the test data are located mostly in the margin area; convex-hulls of both training data do not include most of the test data.

We choose a quantum feature map that embeds data (x_0, x_1) to a single qubit instead of $N = 2$ qubits: $U_{\phi(x_0, x_1)} = R_z(x_1)R_y(x_0)$. Features x_0 and x_1 are latitude and longitude of a Bloch sphere. We use two qubits (q_0 and q_1) *RealAmplitude*⁴² PQC as ansatz: $V(\boldsymbol{\theta}) = R_y^{q_0}(\theta_2) \otimes R_y^{q_1}(\theta_3) CNOT_{q_0 \rightarrow q_1} R_y^{q_0}(\theta_0) \otimes R_y^{q_1}(\theta_1)$. In this article we used *ibmq_montreal*, which is one of the IBM Quantum Falcon Processors. Due to decoherence error, we have optimized loss and decision circuits. See Method for specific techniques. Simultaneous Perturbation Stochastic Approximation (SPSA) algorithm is selected to optimize $V(\boldsymbol{\theta})$ with fast convergence and robustness on the objective function with noise.^{43,44} The measurement of each circuits are repeated $R = 2^{13}$ times to estimate expectation values, which is the maximum possible option for *ibmq_montreal*. Since *ibmq_montreal* is a cloud-based QPU, queue times take the most part of the total run-time. We therefore reduce the QPU usage by applying warm-start and early-stopping techniques. See Method.

Classification results are shown in Figs. 3b and 3d. Theoretical decision function values are calculated by solving Eq. (9) by convex optimization. Noisy simulation refers to the classical simulation that emulates an actual QPU based on a noise parameter set estimated from a noise measurement at a specific time. Once our quantum circuits are optimized for a specific noise parameter set, noisy simulation would perform better than *ibmq_montreal* in terms of decision values. However, although the scale of decision values is reduced, the classification accuracy of VQASVM on an NISQ device still is acceptable for both toy example data sets, because only the signs of decision values matter. In fact, this applies to most variational quantum binary classifiers that measure a probability or expectation as a decision value. VQASVM performance against depolarizing error are shown in Supplementary Information.

Numerical Simulation

A numerical analysis on VQASVM is investigated for a proof of concept with an experimental investigation on the scaling law. We first check if the loss circuit depth grows linearly proportionally to a training set size. The training data sets with various sizes and dimensions are sampled randomly. Three different quantum feature maps $U_{\phi(\cdot)}$ are tested for this analysis: *ZZFeatureMap*⁸ with all-to-all entanglements and linear entanglements,⁴² and heuristic feature map that we designed to be used for the simulations discussed later. *ZZFeatureMap* is the quantum feature map from Ref. 8, which is widely used for kernel-based learning. The parameterized two-qubit gates in *ZZFeatureMap* can connect all possible first-neighbor pairs of two qubits in an all-to-all complete graph or in a linear graph. Examples of these kernels are shown in Supple-

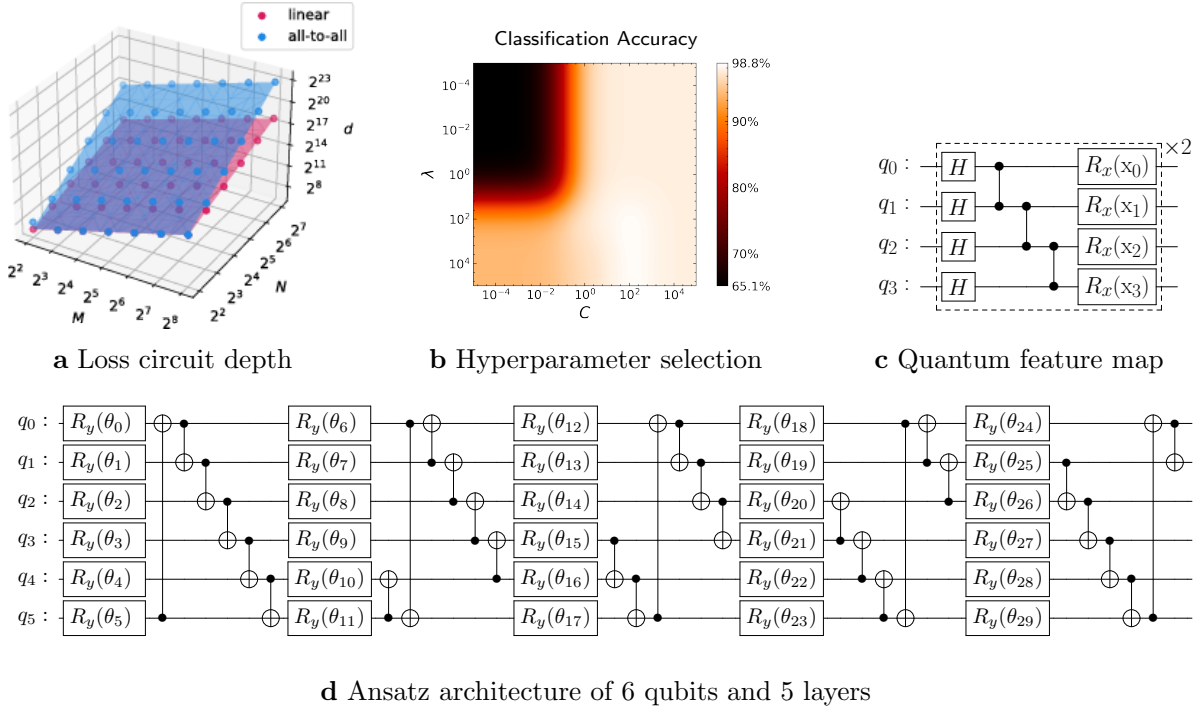


Figure 4: Numerical analyses. **a**, depth of quantum circuit d . The closed circles indicate simulated samples, where transparent planes are the linear fit to them. The results show dependence on M and N . The circuits are decomposed with a universal gate set $\{R_x, R_y, R_z, CNOT\}$. **b**, classification accuracy of iris data set with a $M = 64$ training data set displayed as a function of λ and C . **c**, heuristic quantum feature map used to classify iris data set. **d**, PQC for the ansatz of VQASVM. The number of parameters is $L \times \log(M)$. In this example there are 30 PQC parameters.

mentary Information. Our heuristic kernel-based feature map in Fig. 4c has two repeating layers of parameterized single-qubit gates and controlled- Z acting on first-neighbor qubits. Implementation of $U_{\phi,S}$ follows procedure from Method. A numerical analysis in Fig. 4a shows that the depth of a loss circuit is $d = 2^3 MN (R^2 = 1)$ if there is no parameterized two-qubit gate layer that connects all qubits with all other qubits; otherwise, $d = 2^{1.111} M^{0.991} N^{1.990} (R^2 = 0.999)$. Additionally, we note that the circuit depth of VQASVM is much shorter than that of HHL that is a critical part of LS-QSVM. For example, numerical calculation shows that HHL circuit depth is over 5×10^5 while VQASVM loss circuit depth is only 2^{10} for an 8×8 kernel matrix.

We investigate the performance of VQASVM for classification against a standard data test set, *iris flower data set*,⁴⁵ which is broadly used for bench marking machine learning performance. This consists of 3 classes (iris setosa, iris versicolour, and iris virginica) and 4 features (sepal width, sepal length, petal width, and petal length in cm). In this article, label 1 is assigned to setosa, and label -1 to versicolour and virginica for binary classification. The ranges of features are scaled to $[-\pi, \pi]$.

In this setting, the combination of a heuristic quantum feature map in Fig. 4c for and $U_{\phi(\cdot)}$ can well separate iris flower data. One of supporting evidence is that the singular values of the resulting kernel matrix decay exponentially. The sum of three largest singular values

reaches 42.3% of the total sum of 150 singular values meaning that the mapped data can be well-clustered into three groups of the iris classes. Although other quantum feature map architecture can perform better, we conclude the heuristic feature map is good enough in a numerical analysis. We randomly sampled 64 data to form a training data set and the rest as the test data set. Eq. (9) is numerically analyzed in this case with convex optimization to directly obtain $\boldsymbol{\alpha}^*$ in order to exclude effects of approximation from ansatz $V(\boldsymbol{\theta})$. The result of VQASVM accuracy against λ and C varying from 10^{-4} to 10^4 is shown in Fig. 4b. Although the best values for λ and C differ due to random sampling, the accuracy decreases when both λ and C are small, which can be understood from the previous section on bias regularization. The accuracy of iris data classification is 98.8% with a right choice of hyperparameters. We advice to choose $\lambda \gg 1$ or $C \gg 1$.

Finally, we train and test the whole entity of the VQASVM algorithm to investigate influence of ansatz. The quantum feature map and data set are the same as the previous simulation. We have tested 19 different PQC circuit designs for ansatz $V(\boldsymbol{\theta})$ with varying the number of layers from 1 to 15 for ansatz. Training sets of size $M = 64$ and $M = 128$ are tested and we find that the circuit design shown in Fig. 4d is particularly suitable for the VQASVM algorithm. Refer to Ref. 35 and Supplementary Information for the specific designs of 19 different circuit architectures and their corresponding VQASVM simulation results, respectively.

SPSA is used for the optimizer as it achieves rapid computation in each iteration. We define an objective as residual loss of training, $\Delta = \mathcal{L}_{\phi,\lambda}(\boldsymbol{\theta}^t; \mathcal{S}) + C^{-1}\mathcal{R}(\boldsymbol{\theta}^t) - \tilde{d}^*$ at iteration t . Here \tilde{d}^* from Eq. (9) denotes the minimum of the theoretical loss for a given training data set.

Because of the limited size of the test data set, the resolution of accuracy evaluation is poor, and we adopt the average error of decision function $\mathcal{E} = \frac{1}{|\mathcal{D}|} \sum_{\hat{\mathbf{x}} \in \mathcal{D}} |f_{\phi,\lambda}(\hat{\mathbf{x}}; \boldsymbol{\theta}^t, \mathcal{S}) - h(\hat{\mathbf{x}})|$ as the accuracy measure. This is used to evaluate performance given the set of test data \mathcal{D} and true decision function $h(\cdot)$ that is the argument of sgn of Eq. (10). Figs. 5a and 5b show the convergence and accuracy on the effective number of parameters normalized by training set size, respectively. Both Δ and \mathcal{E} saturate to their minima even when the number of parameters is less than the training set size. We find that $\Delta \sim \mathcal{E}$ due to the similarity between loss and decision functions, as shown in Figs. 5a and 5b. In conclusion, the numerical analysis shows that it is possible for VQASVM with degree of freedom $< M$ to perform as well as VQASVM with a full degree of freedom (i.e. M) in terms of training loss and accuracy, and the convergence is faster in time.

So far we have investigate numerical evaluations of exact models on $\mathcal{L}_{\phi,\lambda}$, \mathcal{R} , and $f_{\phi,\lambda}$. However, in real applications with a quantum machine, there are statistical errors due to a finite number of samplings of quantum measurements in the read-out process. In order to achieve a given error ϵ , measurements should be repeated $R = \mathcal{O}(1/\epsilon^2)$ times. The classification with an exact loss function value can be attained with $R = \infty$.

We perform numerical simulations to confirm that our VQASVM variational algorithm converges even in the presence of a statistical noise. We used the same VQASVM scheme with $M = 64$ training data set and the ansatz in Fig. 4d, which is optimized through 2^{13}

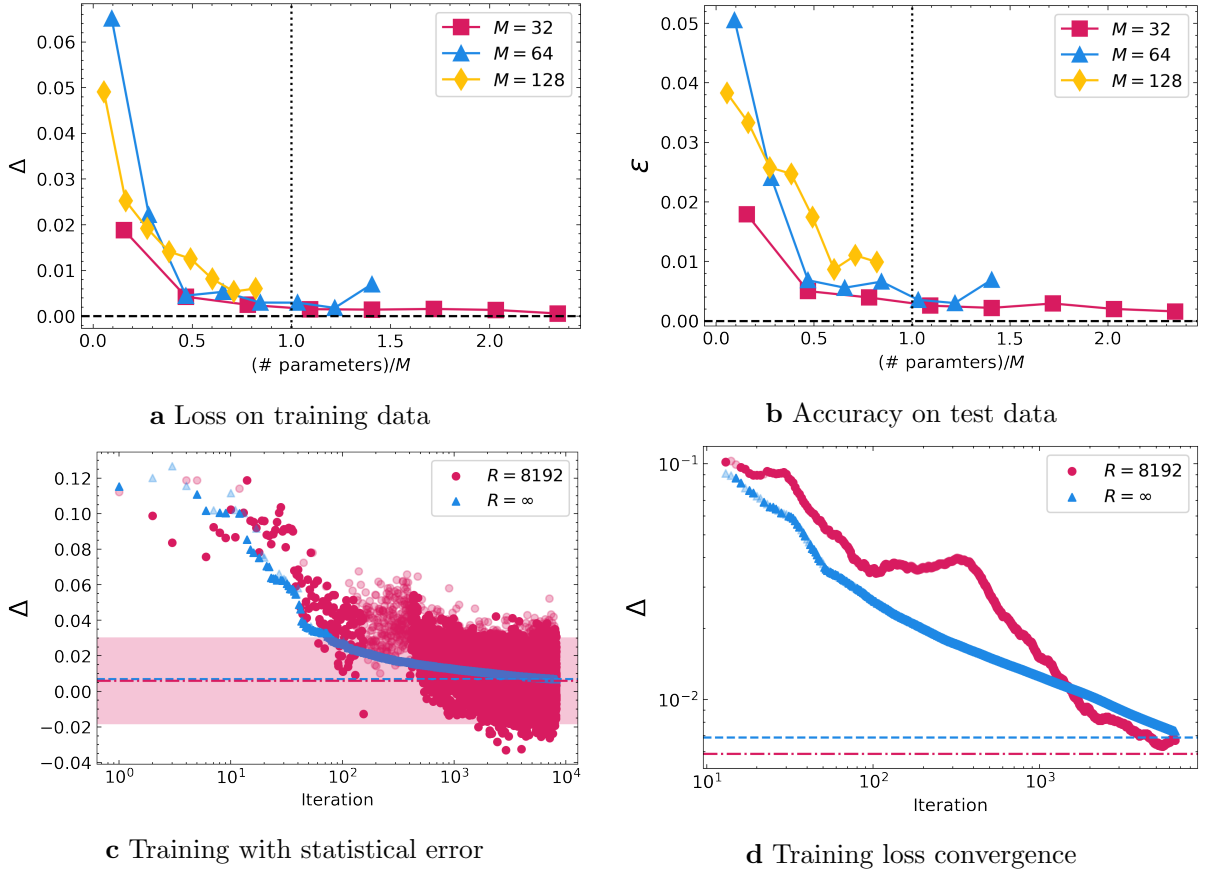


Figure 5: Numerical Analysis on iris data set ($\lambda = C = 10^4$). In **a** and **b**, after 2^{10} iterations, the residual loss of training Δ and average decision value error \mathcal{E} are plotted as a function of normalized number of parameters with respect to M , respectively. In **c** and **d**, the final Δ for $R = 2^{13}$ (blue dashed line) is almost equal to the case of $R = \infty$ (red dot-dashed line). The red shaded area represents 95% credible intervals of last 16 residual losses for $R = 2^{13}$. In **c**, shaded circles and triangles show the convergence of residual losses. See [Method](#). In **d**, coarse-grained Δ averaged over $10^{-0.1}t$ to $10^{0.1}t$ at iteration t is shown in a log scale plot.

iterations with and without statistical errors from the same initial parameters for θ . The convergence results are shown in Fig. 5c. Although having some uncertainty, the result shows that SPSA converges to a local minimum no despite of the statistical error. For a more concrete argument, we eliminate fluctuation of Δ by coarse-graining, as shown in Fig. 5d. Despite some inconsistency, the result shows the convergence rule $\Delta \sim 1/t$ for sufficiently large t regardless of statistical errors, and therefore indicates that VQASVM can be achieved within a finite number of measurements R . Note that it is expected for the SPSA algorithm to converge to a minimum after $t = \mathcal{O}(d/\delta)$ iterations with accuracy δ for d number of free parameters.^{43,44} \mathcal{E} for both cases are equally acceptable: 0.0109 for $R = \infty$ and 0.0114 ± 0.0010 for $R = 2^{13}$ measurements.

Although the above simulation shows that the number of parameters required for certain \mathcal{E} can be reduced to less than M , there are not enough data points to clarify the asymptotic order due to a limited size of the iris data set. We can overcome this limit by adopting the *MNIST data set*. For data preprocessing, 28×28 binary image data of the digit ‘0’ and ‘1’

are selected for binary classification, which features are then reduced to 10 exploiting Principle Component Analysis(PCA). Since the total number of available data for training and test data is 14780 with this preprocessing, we have managed to observe an asymptotic behavior of VQASVM from $M = 2^6$ to $M = 2^{13}$. Two-layer *ZZFeatureMap* with linear entanglements is used as the quantum feature map for the simulation. We observed changes of \mathcal{E} calculated from 2^{13} test data by setting the number of layers for PQC as 1, 3, \dots , 19. *ADAM* optimization with 2^{10} iterations at a learning rate of 0.001 is used to train the VQASVM models. The number of parameters fitted from numerical simulation turns out to have a sub-linear growth on M given some small \mathcal{E} regardless on the design of the ansatz. For instance, the asymptotic order of the number of parameters from the simulation with $\mathcal{E} = 0.00244$ is $\mathcal{O}(M^{0.542})$ with the coefficient of determination $R^2 = 0.971$, or $\mathcal{O}(\log(M)^{3.472})$ with $R^2 = 0.950$. (See Supplementary Information) In other words, the numerical simulation strongly indicates that the empirical run-time complexity of VQASVM is sub-quadratic (i.e. $\mathcal{O}(M^{1.5})$ or $\mathcal{O}(M \text{polylog}(M))$), which is lower than that of classical SVM solvers.

Discussion

In this work, we propose a novel quantum-classical hybrid supervised machine learning algorithm that allows for direct implementation of quadratic programming of support vector machine. The conventional SVM is translated to equivalent quadratic optimization problem which can be solve asymptotically faster in training data set size using variational quantum algorithm. The main idea of our VQASVM algorithm is to encode optimization parameters that represent normalized weight for each training data into a quantum state using less number of parameters. The objective function is evaluated in quantum processors and the parameters are updated based on observed values to minimize objective function in classical processors. The decision function for classification is also evaluated in quantum processors. We have logically and numerically showed that the run-time complexities of loss and decision circuits are $\mathcal{O}(MN)$. We have also numerically justified the PQC approximation; the training loss and accuracy saturate to the theoretical values even with the number of parameters less than the number of training data. We have numerically confirmed convergence and feasibility of VQASVM even with the presence of measurement statistical error using SPSA. We have also verified the sub-quadratic asymptotic run-time complexity of VQASVM numerically. Finally, VQASVM have been tested on cloud-based NISQ processors with a toy example data set to highlight a practical application potential.

From the numerical simulations, we have noticed that expressibility³⁵ of the ansatz is clearly related to VQASVM performance. Accuracy on decision function \mathcal{E} improves when PQC becomes more expressive. See Supplementary Information. Intuitively, it is natural since the effective searching space would be larger for better expressibility. However, circuit #15, which is the PQC architecture shown in Fig. 4d, results in the lowest \mathcal{E} despite a relatively poor expressibility. We speculate that the periodic and circular connections of qubits shown in

Fig. 4d is responsible for such good performance with VQASVM. In theory, the index of training data should not matter; mixing training data by shifting the qubit index order of ansatz (i.e. $q_0q_1 \cdots q_{m-1} \mapsto q_{m-1}q_0 \cdots q_{m-2}$) should not change performance of VQASVM. For Circuit #15, qubit shifting does not alter original architecture critically. After all, our observation on the ansatz designs and their performance in VQASVM does not provide a comprehensive understanding yet, and leaves room for future studies.

The number of PQC parameters is critical to guarantee the performance. Although VQASVM have freedom to choose upto $\mathcal{O}(M)$ number of parameters using hardware-efficient ansatz, we can choose a PQC design with $\mathcal{O}(\text{polylog}(M))$ parameters at the cost of accuracy or training loss performance degradation.³⁷ Taking this as an assumption with a given accuracy bound of ϵ , the training time complexity of VQASVM drops to $\mathcal{O}(MN \text{polylog}(M)/\epsilon)$, suggesting potential asymptotic speed-up compared to SVM. Our numerical experiments with various PQC designs³⁵ show an interesting observation that the number of parameters can be smaller than the number of training data as shown in Figs. 5a and 5b.

VQASVM has an outstanding feature of just few qubit read-out measurements. Only three qubits (a , y_0 , and y_1 in Fig. 1a), and only two qubits (a and y in Fig. 1c) are required to be measured to evaluate the loss function and the decision functions, respectively. In this case, the read-out qubits can be assigned away from one another in the qubit network topology in the real space, in order to minimize the measurement crosstalk.⁴⁶ There can be other error mitigation schemes that can take the advantage of requiring only few qubit measurements. We notice that this is one of the reasons why our experiment on IBM Quantum processors have been successful with only measurement readout error mitigation with no quantum error mitigation. Although this argument is not applicable to regularization circuit, it would not be the problem since the circuit is very simple and regularization terms are less important than the loss term.

VQASVM can be further enhanced with kernel optimization. Like other quantum kernel-based methods, choice of the quantum feature map is crucial for VQASVM. A quantum feature map can be optimized simultaneously while training.⁴⁷ This can be realized in VQASVM with additional steps. Given $U_{\phi(\cdot)}$ can be tuned with some parameters φ , (θ^*, φ) that maximizes the margin should be saddle-point: $(\theta, \varphi) = \arg \min_{\theta} \max_{\varphi} \mathcal{L}_{\phi[\varphi], \lambda}(\theta) + C^{-1} \mathcal{R}(\theta)$. We leave this investigation for future works. Another method to improve VQASVM is boosting. Adopting PQC encoding for the probability vector, VQASVM is not completely a convex problem and may depend on an initial point. In addition, VQASVM can suffer from an overfitting problem, as well as other kernel-based algorithms. In this case, boosting algorithm can be applied to improve test accuracy, by cascading low-performance VQASVMs. Since each VQASVM model only requires $\mathcal{O}(\log(M) + N)$ space, ensemble methods such as boosting are suitable for VQASVM.

Method

Proof of Eqs. (15) and (16)

We first note that a SWAP test operation ($H_a \cdot \text{cSWAP}_{a \rightarrow b, c} \cdot H_a$) in Fig. 1 measures a Hilbert-Schmidt inner product between two pure states by estimating $\langle \sigma_z^a \rangle = |\langle \phi | \psi \rangle|^2$ where a is a control qubit and $|\phi\rangle$ and $|\psi\rangle$ are states on target qubits b and c , respectively. Quantum registers i and j in Fig. 1 are traced out since measurements are performed on only a and y qubits. A reduced density matrix on x and y quantum registers before controlled-SWAP operation is $\rho_{x,y} = \sum_{i=0}^{M-1} \alpha_i |\phi(\mathbf{x}_i)\rangle \langle \phi(\mathbf{x}_i)| \otimes |y_i\rangle \langle y_i|$, which is the statistical sum of quantum states $|\phi(\mathbf{x}_i)\rangle \otimes |y_i\rangle$ with probability α_i .

Let us first consider decision circuit (Fig. 1c). Given that the state $|\phi(\mathbf{x}_i)\rangle_x \otimes |y_i\rangle_y$ and $|\phi(\hat{\mathbf{x}})\rangle_{\hat{x}}$ are prepared, $\langle \mathcal{A}_{a \rightarrow x, \hat{x}} \sigma_z^y \rangle = \langle \mathcal{A}_{a \rightarrow x, \hat{x}} \rangle \langle \sigma_z^y \rangle = y_i \langle \mathcal{A}_{a \rightarrow x, \hat{x}} \rangle$ due to separability. Here, $\mathcal{A}_{a \rightarrow x, \hat{x}}$ can be $(H_a \cdot \text{cSWAP}_{a \rightarrow x, \hat{x}} \cdot H_a)^\dagger \sigma_z^a (H_a \cdot \text{cSWAP}_{a \rightarrow x, \hat{x}} \cdot H_a)$ or $\frac{1}{\lambda} \sigma_a^0$. Similarly, for loss circuit (Fig. 1a), we have states $|\phi(\mathbf{x}_i)\rangle_{x_0} \otimes |y_i\rangle_{y_0}$ and $|\phi(\mathbf{x}_j)\rangle_{x_1} \otimes |y_j\rangle_{y_1}$ with probability $\alpha_i \alpha_j$ so that $\langle \mathcal{A}_{a \rightarrow x_0, x_1} \sigma_z^{y_0} \sigma_z^{y_1} \rangle = \langle \mathcal{A}_{a \rightarrow x_0, x_1} \rangle \langle \sigma_z^{y_0} \sigma_z^{y_1} \rangle = y_i y_j \langle \mathcal{A}_{a \rightarrow x_0, x_1} \rangle$. Therefore, from definition of our quantum kernel, each terms in Eqs. (15) and (16) matches with Eqs. (11) and (13). More direct proof is provided in Ref. 10, 11 and Supplementary Information.

Realization of Quantum Circuits

In this article, $\mathcal{U}_{\phi, \mathcal{S}}$ has been realized using uniformly-controlled one-qubit gates, which require at most $M - 1$ CNOT gates, M one-qubit gates, and a single diagonal $(\log(M) + 1)$ -qubit gate.^{33,48} We have compiled the quantum feature map with a basis gate set composed of Pauli rotations and CNOT. $\mathcal{U}_{\phi, \mathcal{S}}$ can be efficiently implemented by replacing all Pauli rotations with uniformly-controlled Pauli rotations. The training data label embedding of $\mathcal{U}_{\phi, \mathcal{S}}$ can be also easily implemented using a uniformly-controlled Pauli X rotation. (i.e. setting rotation angle as π if label is positive and 0 otherwise.) Although this procedure allows incorporating existing quantum feature maps, the complexity may increase up to $\mathcal{O}(MN^2)$ if the quantum feature map contains all-to-all connecting parameterized two-qubit gates. Still, such $\mathcal{U}_{\phi, \mathcal{S}}$ has linear complexity proportional to the number of training data.

Application to IBM Quantum Processors.

Since IBM quantum processors are based on superconducting qubits, all-to-all connection is not possible. Additional SWAP operations among qubits for distant interactions would shorten the effective decoherence time and increase noise. We have carefully selected physical qubits of *ibmq-montreal* in order to reduced SWAP operations. For $M = 4$ and single qubit embedding, $m = 2$ and $n = 1$. Thus the multi-qubits interaction is required for the following connections: (a, x_0, x_1) , $([i_0, i_1], x_0)$, $([j_0, j_1], x_1)$, $([i_0, i_1], y_0)$, and $([j_0, j_1], y_1)$. We first choose the 9 qubits connected in a linear topology such that the overall estimated single and two-qubit

gate errors are the lowest among other possible options.¹ For instance, the physical qubits indexed 1, 2, 3, 4, 5, 8, 11, 14, and 16 in *ibmq_montreal* have been selected in this article, which is visualized in Supplementary Information. We then assign virtual qubit in the order of $y_0, i_0, i_1, x_0, a, x_1, j_0, j_1, y_1$ so that the aforementioned required connections can be made between qubits next to each others. In conclusion, the mapping from virtual qubits to physical qubits is $\{a \mapsto 5, i_0 \mapsto 2, i_1 \mapsto 1, x_i \mapsto 3, y_i \mapsto 4, j_0 \mapsto 11, j_1 \mapsto 14, x_j \mapsto 8, y_j \mapsto 16\}$ in this experiment. We report that with this arrangement, circuit depths of loss and decision circuits are 60 and 59 for the balanced data set and 64 and 63 for the unbalanced data set, in the basis gate set of *ibmq_montreal*: $\{R_z, \sqrt{X}, X, CNOT\}$.

Additional Techniques on SPSA

The conventional SPSA algorithm has been adjusted for faster and better convergence. First, *blocking* technique has been introduced. Assuming variance σ^2 of objective function $\mathcal{L}_{\phi, \lambda} + C^{-1}\mathcal{R}$ is uniform on parameter θ , the next iteration $t + 1$ is rejected if $[\mathcal{L}_{\phi, \lambda} + C^{-1}\mathcal{R}](\theta^{t+1}) \geq [\mathcal{L}_{\phi, \lambda} + C^{-1}\mathcal{R}](\theta^t) + 2\sigma$. SPSA would converge faster with blocking by preventing its objective function from getting too large with some probability (See Supplementary Information). Second, *Early-stopping* has been applied. Iteration is terminated if some conditions are satisfied. Specifically, we stop SPSA optimization if the average of last 16 recorded training loss values is greater than or equal to last 32 recorded values. Early stopping has reduced training time drastically, especially running on QPU. Last, we have averaged last 16 recorded parameters to yield result: $\theta^* = \frac{1}{16} \sum_{i=0}^{15} \theta^{t-i}$. Combination of these techniques have been selected for better optimization. We adopted all of these techniques for experiments and simulations as default.

Warm-start optimization

We report cases that optimization of the IBM Q Quantum Processors yields vanishing kernel amplitudes due to a constantly varying error map problem. The total run time should be minimized to avoid this problem. Since accessing QPU takes a relatively long queue time, we apply a ‘warm-start’ technique, which reduces number of QPU uses. We first initialize and proceed a few iterations (32) with noisy simulation on CPU and then evaluate functions on QPU for the rest of the iterations. Note that an SPSA optimizer requires heavy initialization computation such as for calculating an initial variance. With this warm-start method, we were able to obtain better results on some trials.

References

- [1] Sharma, K. *et al.* Reformulation of the No-Free-Lunch Theorem for Entangled Datasets. *Physical Review Letters* **128**, 070501 (2022). URL <https://link.aps.org/doi/10.1103/PhysRevLett.128.070501>.

¹The noise parameters and topology of *ibmq_montreal* are provided by IBM Quantum.

- [2] Lloyd, S., Mohseni, M. & Rebentrost, P. Quantum algorithms for supervised and unsupervised machine learning. *arXiv preprint* (2013). URL <http://arxiv.org/abs/1307.0411>.
- [3] Biamonte, J. *et al.* Quantum machine learning. *Nature* **549**, 195–202 (2017). URL <http://www.nature.com/articles/nature23474>.
- [4] Schuld, M. & Petruccione, F. *Supervised Learning with Quantum Computers*. Quantum Science and Technology (Springer International Publishing, Cham, 2018). URL <https://link.springer.com/10.1007/978-3-319-96424-9>.
- [5] Rebentrost, P., Mohseni, M. & Lloyd, S. Quantum Support Vector Machine for Big Data Classification. *Physical Review Letters* **113**, 130503 (2014). URL <https://link.aps.org/doi/10.1103/PhysRevLett.113.130503>.
- [6] Schuld, M., Fingerhuth, M. & Petruccione, F. Implementing a distance-based classifier with a quantum interference circuit. *EPL (Europhysics Letters)* **119**, 60002 (2017). URL <https://iopscience.iop.org/article/10.1209/0295-5075/119/60002>.
- [7] Schuld, M. & Killoran, N. Quantum Machine Learning in Feature Hilbert Spaces. *Physical Review Letters* **122**, 040504 (2019). URL <https://link.aps.org/doi/10.1103/PhysRevLett.122.040504>.
- [8] Havlíček, V. *et al.* Supervised learning with quantum-enhanced feature spaces. *Nature* **567**, 209–212 (2019). URL <http://www.nature.com/articles/s41586-019-0980-2>.
- [9] Lloyd, S., Schuld, M., Ijaz, A., Izaac, J. & Killoran, N. Quantum embeddings for machine learning. *arXiv preprint* (2020). URL <http://arxiv.org/abs/2001.03622>.
- [10] Blank, C., Park, D. K., Rhee, J.-K. K. & Petruccione, F. Quantum classifier with tailored quantum kernel. *npj Quantum Information* **6**, 41 (2020). URL <http://www.nature.com/articles/s41534-020-0272-6>.
- [11] Park, D. K., Blank, C. & Petruccione, F. The theory of the quantum kernel-based binary classifier. *Physics Letters A* **384**, 126422 (2020). URL <https://linkinghub.elsevier.com/retrieve/pii/S0375960120302541>.
- [12] Schuld, M. Supervised quantum machine learning models are kernel methods. *arXiv preprint* (2021). URL <http://arxiv.org/abs/2101.11020>.
- [13] Liu, Y., Arunachalam, S. & Temme, K. A rigorous and robust quantum speed-up in supervised machine learning. *Nature Physics* **17**, 1013–1017 (2021). URL <https://www.nature.com/articles/s41567-021-01287-z>.
- [14] Blank, C., da Silva, A. J., de Albuquerque, L. P., Petruccione, F. & Park, D. K. Compact quantum distance-based binary classifier. *arXiv preprint* (2022). URL <http://arxiv.org/abs/2202.02151>.

- [15] Cortes, C. & Vapnik, V. Support-vector networks. *Machine Learning* **20**, 273–297 (1995). URL <http://link.springer.com/10.1007/BF00994018>.
- [16] Boser, B. E., Guyon, I. M. & Vapnik, V. N. A training algorithm for optimal margin classifiers. In *Proceedings of the fifth annual workshop on Computational learning theory*, 144–152 (1992).
- [17] Vapnik, V., Golowich, S. E. & Smola, A. Support vector method for function approximation, regression estimation, and signal processing. In *Advances in Neural Information Processing Systems*, 281–287 (1997).
- [18] Guyon, I., Vapnik, V., Boser, B., Bottou, L. & Solla, S. Capacity control in linear classifiers for pattern recognition. In *Proceedings., 11th IAPR International Conference on Pattern Recognition. Vol.II. Conference B: Pattern Recognition Methodology and Systems*, 385–388 (IEEE Comput. Soc. Press, 1992). URL <http://ieeexplore.ieee.org/document/201798/>.
- [19] Steinwart, I. & Christmann, A. *Support vector machines* (Springer Science & Business Media, 2008).
- [20] Giuntini, R. *et al.* Quantum State Discrimination for Supervised Classification. *arXiv preprint* (2021). URL <http://arxiv.org/abs/2104.00971>.
- [21] Harrow, A. W., Hassidim, A. & Lloyd, S. Quantum Algorithm for Linear Systems of Equations. *Physical Review Letters* **103**, 150502 (2009). URL <https://link.aps.org/doi/10.1103/PhysRevLett.103.150502>.
- [22] Lloyd, S., Mohseni, M. & Rebentrost, P. Quantum principal component analysis. *Nature Physics* **10**, 631–633 (2014). URL <http://www.nature.com/articles/nphys3029>.
- [23] Aaronson, S. Read the fine print. *Nature Physics* **11**, 291–293 (2015). URL <http://www.nature.com/articles/nphys3272>.
- [24] Preskill, J. Quantum Computing in the NISQ era and beyond. *Quantum* **2**, 79 (2018). URL <https://quantum-journal.org/papers/q-2018-08-06-79/>.
- [25] Boyd, S. P. & Vandenberghe, L. *Convex optimization* (Cambridge university press, 2004).
- [26] Coppersmith, D. & Winograd, S. Matrix multiplication via arithmetic progressions. *Journal of Symbolic Computation* **9**, 251–280 (1990). URL <https://linkinghub.elsevier.com/retrieve/pii/S0747717108800132>.
- [27] Chang, C.-C. & Lin, C.-J. LIBSVM. *ACM Transactions on Intelligent Systems and Technology* **2**, 1–27 (2011). URL <https://dl.acm.org/doi/10.1145/1961189.1961199>.

- [28] Deisenroth, M. P., Faisal, A. A. & Ong, C. S. *Mathematics for Machine Learning* (Cambridge University Press, 2020). URL <https://www.cambridge.org/highereducation/books/mathematics-for-machine-learning/5EE57FD1CFB23E6EB11E130309C7EF98#contents>.
- [29] Mangasarian, O. & Musicant, D. Successive overrelaxation for support vector machines. *IEEE Transactions on Neural Networks* **10**, 1032–1037 (1999). URL <http://ieeexplore.ieee.org/document/788643/>.
- [30] Frie\ss, T.-T., Cristianini, N. & Campbell, C. The Kernel-Adatron Algorithm: A Fast and Simple Learning Procedure for Support Vector Machines. In *Proceedings of the Fifteenth International Conference on Machine Learning, ICML '98*, 188–196 (Morgan Kaufmann Publishers Inc., San Francisco, CA, USA, 1998).
- [31] Hsu, C.-W. & Lin, C.-J. A Simple Decomposition Method for Support Vector Machines. *Machine Learning* **46**, 291–314 (2002). URL <https://doi.org/10.1023/A:1012427100071>.
- [32] Chih-Wei Hsu & Chih-Jen Lin. A comparison of methods for multiclass support vector machines. *IEEE Transactions on Neural Networks* **13**, 415–425 (2002). URL <http://ieeexplore.ieee.org/document/991427/>.
- [33] Mottonen, M., Vartiainen, J. J., Bergholm, V. & Salomaa, M. M. Transformation of quantum states using uniformly controlled rotations. *arXiv preprint* (2004). URL <http://arxiv.org/abs/quant-ph/0407010>.
- [34] Araujo, I. F., Park, D. K., Petruccione, F. & da Silva, A. J. A divide-and-conquer algorithm for quantum state preparation. *Scientific Reports* **11**, 6329 (2021). URL <https://doi.org/10.1038/s41598-021-85474-1><http://www.nature.com/articles/s41598-021-85474-1>.
- [35] Sim, S., Johnson, P. D. & Aspuru-Guzik, A. Expressibility and Entangling Capability of Parameterized Quantum Circuits for Hybrid Quantum-Classical Algorithms. *Advanced Quantum Technologies* **2**, 1900070 (2019). URL <https://onlinelibrary.wiley.com/doi/10.1002/qute.201900070>.
- [36] Kandala, A. *et al.* Hardware-efficient variational quantum eigensolver for small molecules and quantum magnets. *Nature* **549**, 242–246 (2017). URL <https://doi.org/10.1038/nature23879>.
- [37] Farhi, E., Goldstone, J. & Gutmann, S. A Quantum Approximate Optimization Algorithm. *arXiv preprint* 1–16 (2014). URL <http://arxiv.org/abs/1411.4028>.
- [38] Cerezo, M. *et al.* Variational quantum algorithms. *Nature Reviews Physics* **3**, 625–644 (2021). URL <https://www.nature.com/articles/s42254-021-00348-9>.

- [39] Mitarai, K., Negoro, M., Kitagawa, M. & Fujii, K. Quantum circuit learning. *Physical Review A* **98**, 032309 (2018). URL <https://link.aps.org/doi/10.1103/PhysRevA.98.032309>.
- [40] Schuld, M., Bergholm, V., Gogolin, C., Izaac, J. & Killoran, N. Evaluating analytic gradients on quantum hardware. *Physical Review A* **99**, 032331 (2019). URL <https://link.aps.org/doi/10.1103/PhysRevA.99.032331>.
- [41] Suykens, J. A. K. & Vandewalle, J. Least Squares Support Vector Machine Classifiers. *Neural Processing Letters* **9**, 293–300 (1999). URL <https://doi.org/10.1023/A:1018628609742>.
- [42] ANIS, M. D. S. *et al.* Qiskit: An Open-source Framework for Quantum Computing (2021).
- [43] Spall, J. C. A one-measurement form of simultaneous perturbation stochastic approximation. *Automatica* **33**, 109–112 (1997).
- [44] Spall, J. Adaptive stochastic approximation by the simultaneous perturbation method. *IEEE Transactions on Automatic Control* **45**, 1839–1853 (2000). URL <http://ieeexplore.ieee.org/document/880982/>.
- [45] Fisher, R. A. & Marshall, M. Iris data set (1936).
- [46] Seo, S. & Bae, J. Measurement Crosstalk Errors in Cloud-Based Quantum Computing. *IEEE Internet Computing* **26**, 26–33 (2022). URL <https://ieeexplore.ieee.org/document/9645257/>.
- [47] Glick, J. R. *et al.* Covariant quantum kernels for data with group structure. *arXiv preprint* (2021). URL <https://arxiv.org/abs/2105.03406>.
- [48] Bergholm, V., Vartiainen, J. J., Möttönen, M. & Salomaa, M. M. Quantum circuits with uniformly controlled one-qubit gates. *Physical Review A* **71**, 052330 (2005). URL <https://link.aps.org/doi/10.1103/PhysRevA.71.052330>.

Acknowledgment

This work was supported by Samsung Research Funding & Incubation Center of Samsung Electronics under Project Number SRFC-TF2003-01. We acknowledge the use of IBM Quantum services for this work. The views expressed are those of the authors, and do not reflect the official policy or position of IBM or the IBM Quantum team.

Author contributions

S.P. contributed to development and experimental verification of the theoretical and circuit models; D.K.P. contributed to developing the initial concept and the experimental verification;

J.K.R. contributed in development and validation of the main concept, and organization of this work. All coauthors contributed in writing the manuscript.

Competing interests

The authors declare no competing interests.

Data Availability

The numerical data generated in this work is available from the corresponding author upon reasonable request. <https://github.com/Siheon-Park/QUIC-Projects>

Variational Quantum Support Vector Machine With Inference Transfer

Siheon Park¹, Daniel K. Park², and June-Koo Kevin Rhee^{*1,3}

¹School of Electrical Engineering and KAIST Institute for IT Convergence, KAIST, Daejeon, Korea

²Dept. of Applied Statistics & Dept. of Statistics and Data Science, Yonsei University, Seoul, Korea

³Qunova Computing, Inc., Deajeon, S. Korea

August 15, 2022

Supplementary Information

A Proof of Eqs. (15) and (16)

The proof of Eqs. (15) is as follows:

$$\begin{aligned}
|\psi\rangle &= \sum_{i=0}^{M-1} \sqrt{\alpha_i} |0, i, \phi(\mathbf{x}_i), y_i, \phi(\hat{\mathbf{x}})\rangle \\
&\Rightarrow \frac{1}{\sqrt{2}} \sum_{i=0}^{M-1} \sqrt{\alpha_i} |0, i, \phi(\mathbf{x}_i), y_i, \phi(\hat{\mathbf{x}})\rangle + \frac{1}{\sqrt{2}} \sum_{i=0}^{M-1} \sqrt{\alpha_i} |1, i, \phi(\mathbf{x}_i), y_i, \phi(\hat{\mathbf{x}})\rangle \\
&\Rightarrow \frac{1}{\sqrt{2}} \sum_{i=0}^{M-1} \sqrt{\alpha_i} |0, i, \phi(\mathbf{x}_i), y_i, \phi(\hat{\mathbf{x}})\rangle + \frac{1}{\sqrt{2}} \sum_{i=0}^{M-1} \sqrt{\alpha_i} |1, i, \phi(\hat{\mathbf{x}}), y_i, \phi(\mathbf{x}_i)\rangle \\
&\Rightarrow \frac{1}{2} \sum_{i=0}^{M-1} \sqrt{\alpha_i} (|0, i, \phi(\mathbf{x}_i), y_i, \phi(\hat{\mathbf{x}})\rangle + |0, i, \phi(\hat{\mathbf{x}}), y_i, \phi(\mathbf{x}_i)\rangle) \\
&\quad + \frac{1}{2} \sum_{i=0}^{M-1} \sqrt{\alpha_i} (|1, i, \phi(\mathbf{x}_i), y_i, \phi(\hat{\mathbf{x}})\rangle - |1, i, \phi(\hat{\mathbf{x}}), y_i, \phi(\mathbf{x}_i)\rangle) \\
&\xrightarrow{\langle Z_a Z_y \rangle} \sum_{i=0}^{M-1} \alpha_i y_i |\langle \phi(\mathbf{x}_i) | \phi(\hat{\mathbf{x}}) \rangle|^2, \quad \xrightarrow{\langle I_a Z_y \rangle} \sum_{i=0}^{M-1} \alpha_i y_i
\end{aligned} \tag{1}$$

The proof of Eqs. (16) is as follows:

$$\begin{aligned}
|\psi\rangle &= \sum_{i,j=0}^{M-1} \sqrt{\alpha_i} \sqrt{\alpha_j} |0, i, \phi(\mathbf{x}_i), y_i, j, \phi(\mathbf{x}_j), y_j\rangle \\
&\Rightarrow \frac{1}{\sqrt{2}} \sum_{i,j=0}^{M-1} \sqrt{\alpha_i} \sqrt{\alpha_j} |0, i, \phi(\mathbf{x}_i), y_i, j, \phi(\mathbf{x}_j), y_j\rangle + \frac{1}{\sqrt{2}} \sum_{i,j=0}^{M-1} \sqrt{\alpha_i} \sqrt{\alpha_j} |1, i, \phi(\mathbf{x}_i), y_i, j, \phi(\mathbf{x}_j), y_j\rangle \\
&\Rightarrow \frac{1}{\sqrt{2}} \sum_{i,j=0}^{M-1} \sqrt{\alpha_i} \sqrt{\alpha_j} |0, i, \phi(\mathbf{x}_i), y_i, j, \phi(\mathbf{x}_j), y_j\rangle + \frac{1}{\sqrt{2}} \sum_{i,j=0}^{M-1} \sqrt{\alpha_i} \sqrt{\alpha_j} |1, i, \phi(\mathbf{x}_j), y_i, j, \phi(\mathbf{x}_i), y_j\rangle \\
&\Rightarrow \frac{1}{2} \sum_{i,j=0}^{M-1} \sqrt{\alpha_i} \sqrt{\alpha_j} (|0, i, \phi(\mathbf{x}_i), y_i, j, \phi(\mathbf{x}_j), y_j\rangle + |0, i, \phi(\mathbf{x}_j), y_i, j, \phi(\mathbf{x}_i), y_j\rangle) \\
&\quad + \frac{1}{2} \sum_{i,j=0}^{M-1} \sqrt{\alpha_i} \sqrt{\alpha_j} (|0, i, \phi(\mathbf{x}_i), y_i, j, \phi(\mathbf{x}_j), y_j\rangle - |0, i, \phi(\mathbf{x}_j), y_i, j, \phi(\mathbf{x}_i), y_j\rangle) \\
&\quad \xrightarrow{\langle Z_a Z_{y_0} Z_{y_1} \rangle} \sum_{i,j=0}^{M-1} \alpha_i \alpha_j y_i y_j |\langle \phi(\mathbf{x}_i) | \phi(\mathbf{x}_j) \rangle|^2, \quad \xrightarrow{\langle I_a Z_{y_0} Z_{y_1} \rangle} \sum_{i,j=0}^{M-1} \alpha_i \alpha_j y_i y_j = \left(\sum_{i=0}^{M-1} \alpha_i y_i \right)^2
\end{aligned} \tag{2}$$

For more detail, see.?,?

B Supplementary Figures

In this section, we provide supplementary figures mentioned in the main text.

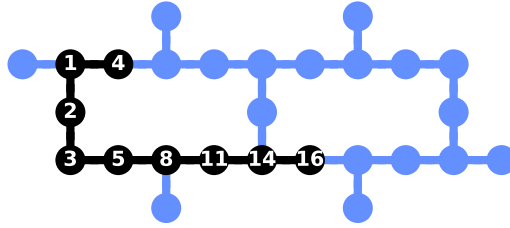


Figure 1: *ibm_montreal* qubits configurations. We used qubits colored in black for QASVM with toy data set

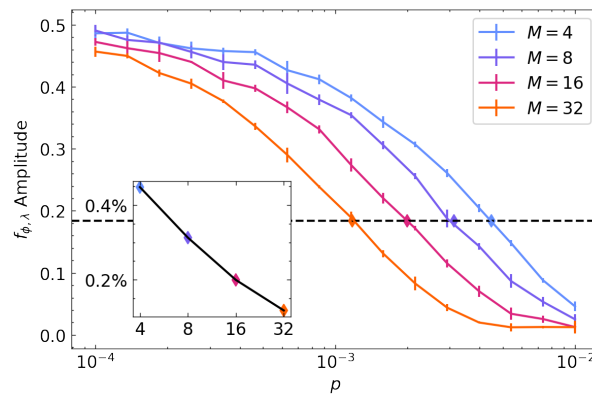
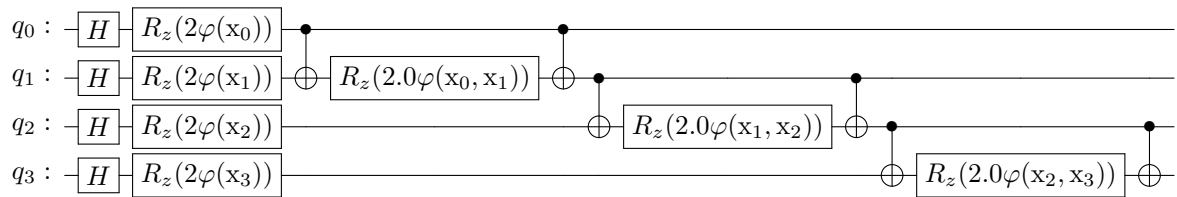
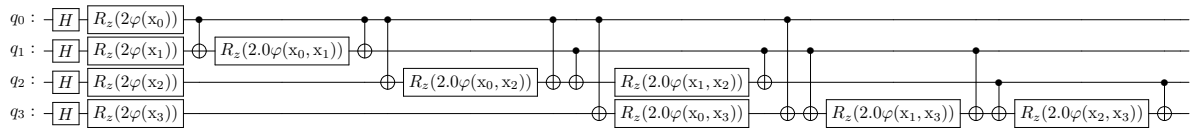


Figure 2: Noise robustness simulation result on depolarizing error. $f_{\phi, \lambda}$ amplitude represents amplitude of sine-fitted function of measured decision values. p is depolarizing error rate of single-qubit gate. We set the error rate of two-qubit gates 10 times higher than that of single-qubit gates.



a *ZZFeatureMap* with linear entanglement



b *ZZFeatureMap* with all-to-all entanglement

Figure 3: Example quantum feature map from Ref.?

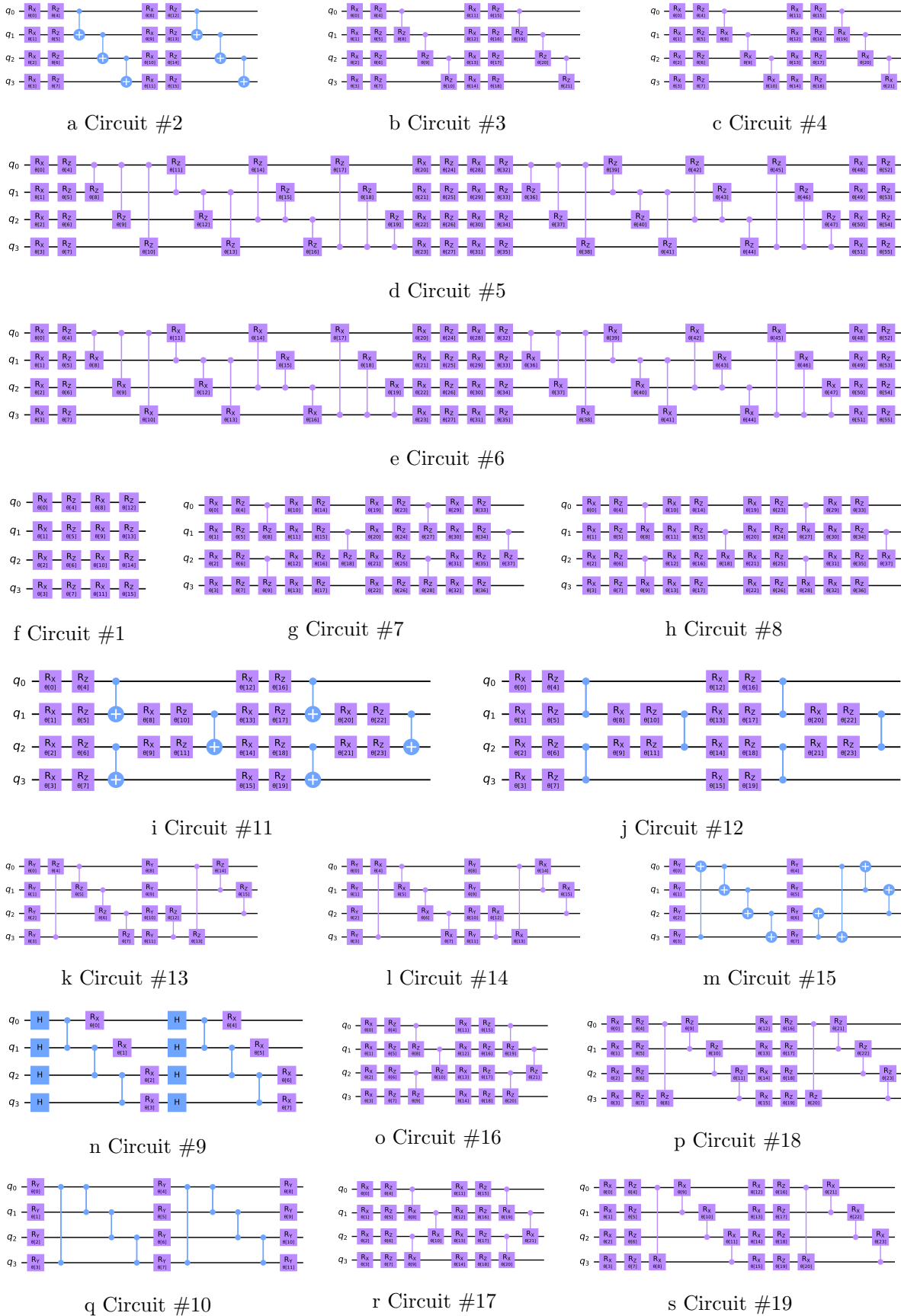


Figure 4: 19 sample PQC architecture provided in Ref. ?. Each circuit has 4 qubits and 2 layers.

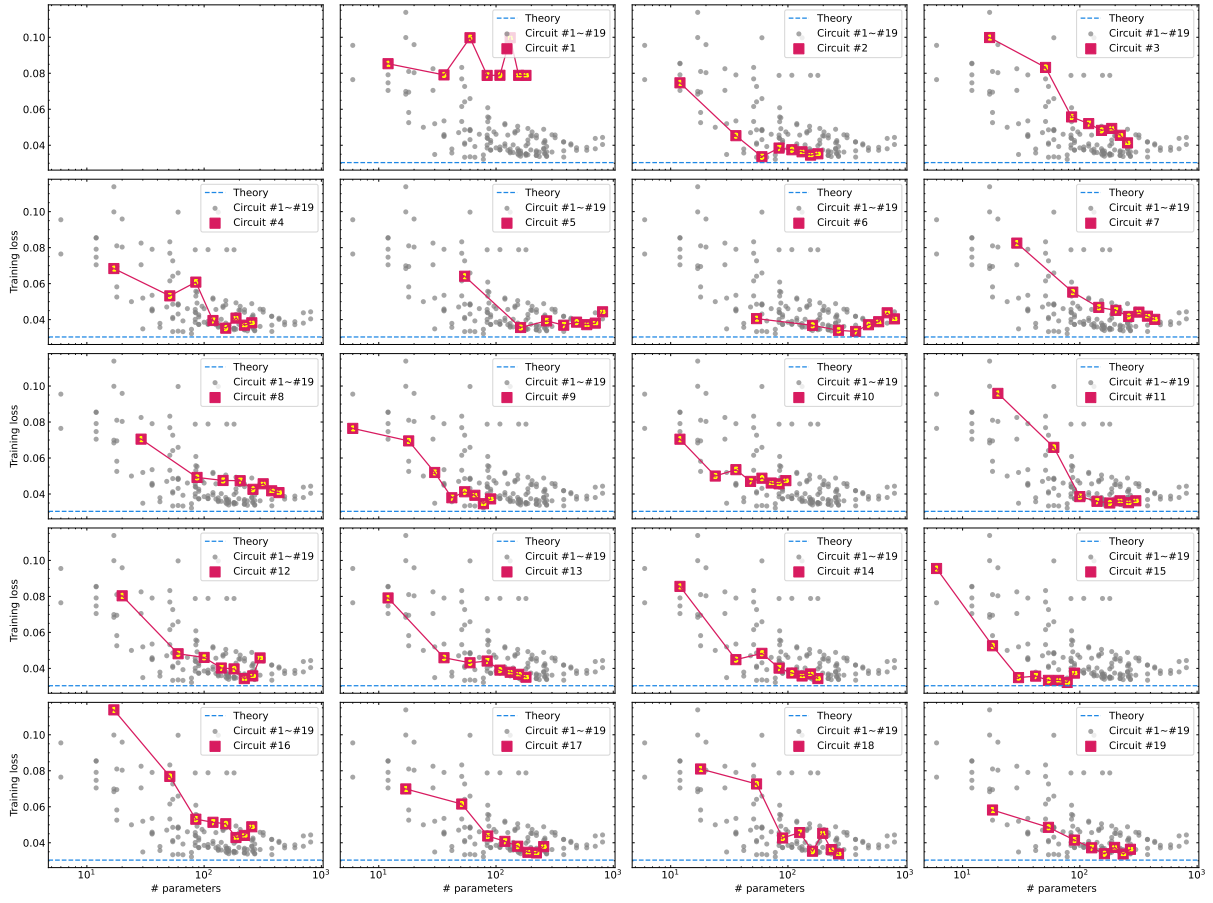


Figure 5: Training results on iris data set ($M = 64$)

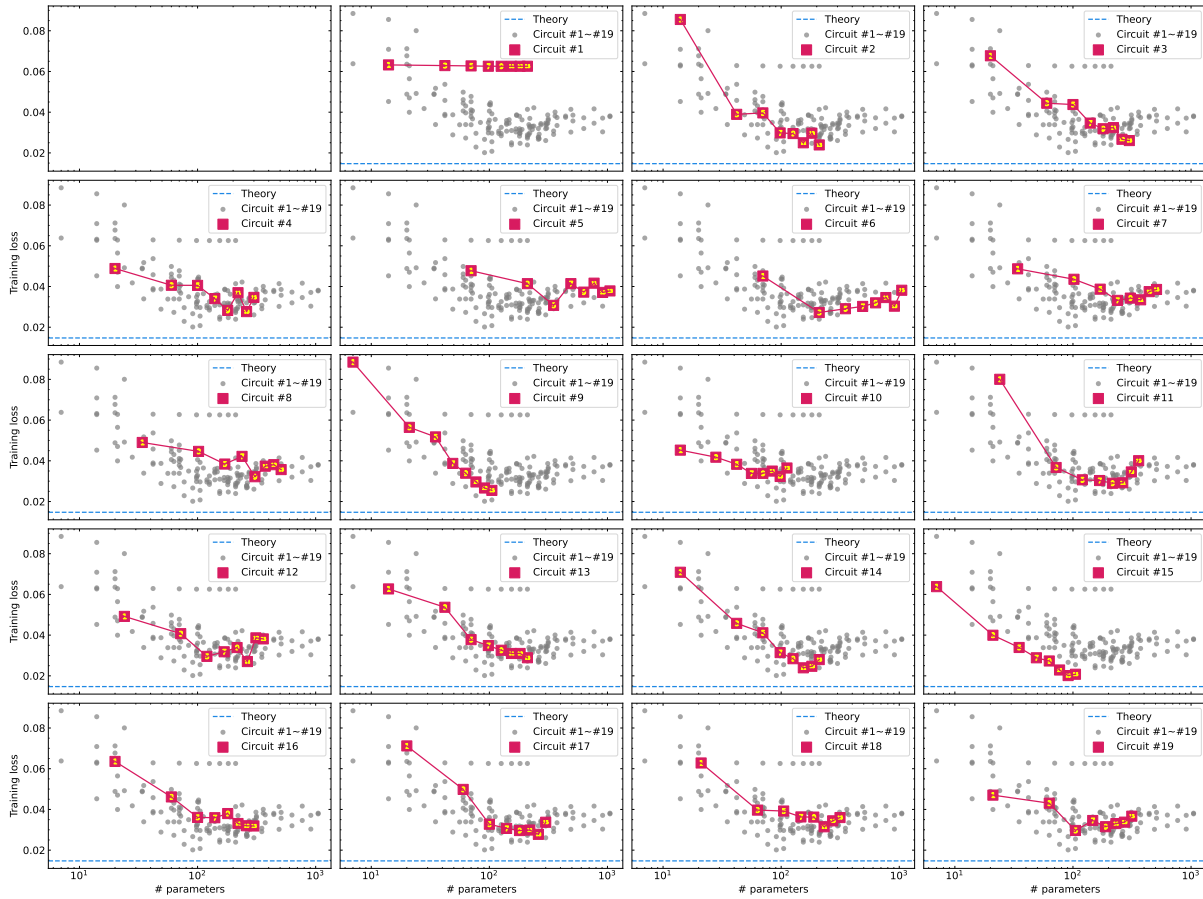
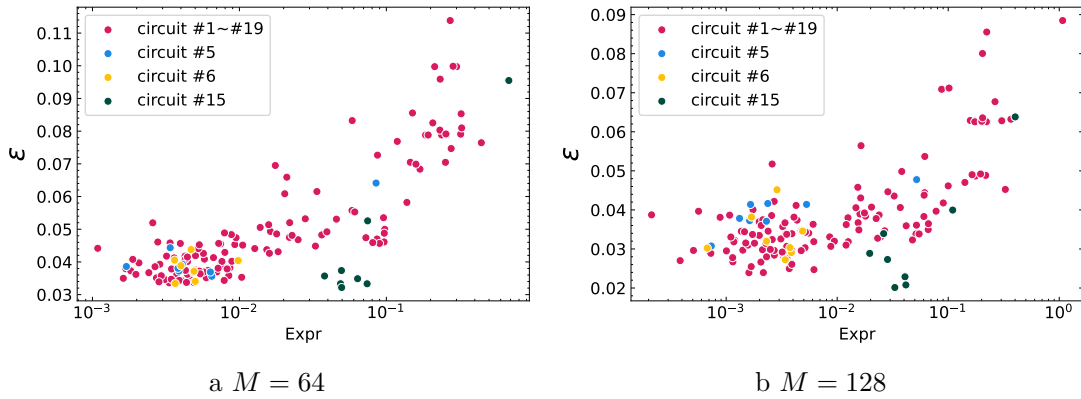


Figure 6: Training results on iris data set ($M = 128$)



a $M = 64$

b $M = 128$

Figure 7: Decision value error on iris data set. Expr refers to expressibility of PQCs.[?] Circuit #5 and #6 has $L \times \log(M)^2$ parameters.

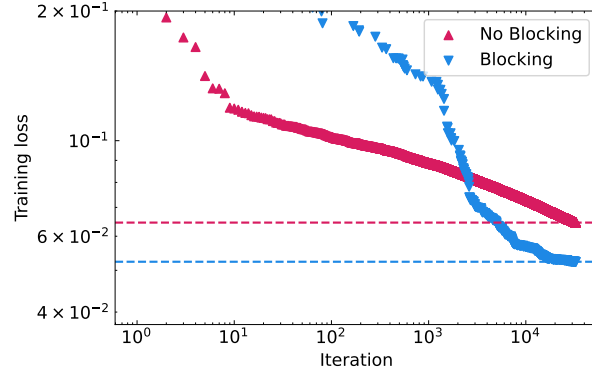
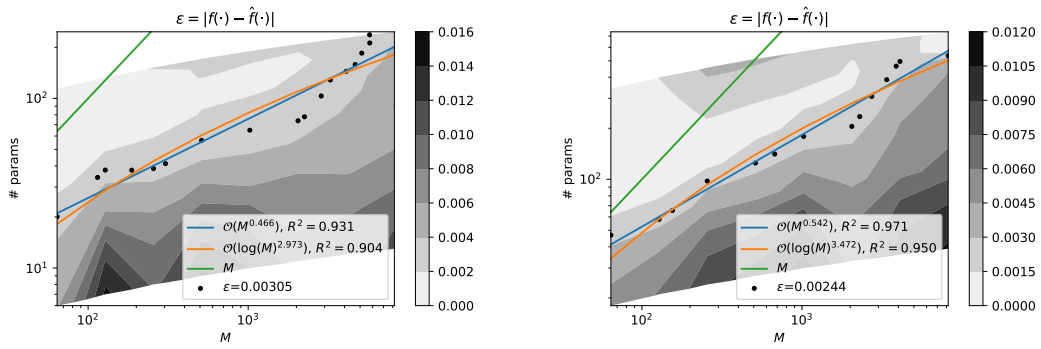


Figure 8: Blocking technique for SPSA. Training loss converges faster when blocking is used.



a *BasicEntanglerLayers* Ansatz

b *StronglyEntanglingLayers* Ansatz

Figure 9: Sublinear growth of number of parameters independent of PQC architecture.